Laboratory of Applied Mechanical Design

Experimental and Numerical Investigation of a Small-Scale Steam Turbine

Semester Project
January 2020

Author :
Diya Achi

Supervisors :
Prof. Jürg Schiffmann
Dr. Patrick Hubert Wagner

This file was downloaded from the institutional repository of EPFL Infoscience
https://infoscience.epfl.ch
http://infoscience.epfl.ch/record/276092

© 2020. This manuscript version is made available under the CC-BY-NC-ND 4.0 license http://creativecommons.org/licenses/by-nc-nd/4.0/

Abstract

This paper focuses on a small-scale radial steam turbine which is part of a fan-turbine unit (FTU) realizing the anode off-gas recirculation of a Solid Oxide Fuel Cell (SOFC). Due to the small size of the turbine (15mm diameter), it is not possible to determine its power by directly measuring the torque. Therefore, the performance parameters are evaluated using thermodynamics. However, heat transfers within the FTU have a non-negligible impact on the evaluation of the turbine power and total-to-total isentropic efficiency.

New temperature and pressure measurements were thus conducted to refine the experimental results and the numerical model. The analysis of the experimental and numerical results highlights the significant influence of heat transfers, and provides a range for the turbine power and total-to-total isentropic efficiency, which are on the order of 34W and 39%, respectively.

Furthermore, a heat investigation was carried out on the FTU in order to localise and determine the heat losses to the environment by using a simplified model. Through investigation, the primary source of heat loss was located at the turbine outlet.

Acknowledgements

I would like to express my deep gratitude to Prof. Jürg Schiffman and Dr. Patrick Wagner for giving me the opportunity to work on this project. I would like to especially thank Dr. Wagner for supervising my work and for his valuable, constructive guidance throughout this semester. I would also like to thank M. Sajjad Zakeralhoseini for his helpful assistance on Computational Fluid Dynamics (CFD) and experimental uncertainties.

Table of Contents

1 Introduction **1**
1.1 Motivation . . . 1
1.2 The technology . . . 1
1.3 Objectives . . . 2

2 Theory **2**
2.1 Power . . . 2
2.2 Total-To-Total Isentropic Efficiency . . . 2
2.3 Degree of Reaction . . . 3

3 Experimental Investigation **3**
3.1 Test and Measurement Setup . . . 3
3.2 Temperature Measurements . . . 7
3.2.1 Cold Air Test . . . 7
3.2.2 Hot Air Test . . . 9
3.3 Methodology . . . 10

4 Numerical Investigation **11**
4.1 Numerical Setup . . . 11
4.2 Boundary Conditions . . . 12
4.3 Method . . . 12

5 Analytical Investigation **13**

6 Results & Discussion **14**
6.1 Cold Air Test . . . 14
6.2 Hot Air Test . . . 16

7 Heat Investigation **19**
7.1 FTU Heat Losses . . . 19
7.1.1 Methodology . . . 19
7.1.2 FTU Model . . . 20
7.1.3 Results & Discussion . . . 22
7.2 Turbine Heat Losses . . . 23
7.2.1 Methodology . . . 23
7.2.2 Results & Discussion . . . 23

8 Conclusion **24**

A Recovery Factor of the Thermocouples **26**

B Mesh Sensitivity **26**

Nomenclature **29**

List of Figures **32**

List of Tables **33**

References **34**

1 | Introduction

1.1 Motivation

With a continuously expanding population, the world is currently facing major issues. In fact, the population growth and development are followed by a rise in the energy consumption. Therefore, the earth's limited resources and its environment are being strained to meet the demands of human kind. An efficient energy management and production is essential in order to sustain our resources. Innovation is thus a necessity in this field.

The developed project targets an efficient as well as a decentralised energy conversion. It is composed of a high efficiency solid oxide fuel cell (SOFC), which produces electricity and heat from natural gas. The distributed energy conversion is also encouraged, limiting the energy losses between the source and the consumers and allowing them to recover the waste heat.

1.2 The technology

The energy is produced using an SOFC. This fuel cell is coupled with a fan-turbine unit (FTU), which realizes the anode off-gas recirculation (AOR). The recirculation will provide a higher global fuel utilization, which results in higher efficiencies of the system, up to 65% [1]. Moreover, the excess heat can be recovered for cogeneration. The turbine of the FTU is the main focus of this project.

The Turbine The studied turbine is a small-scale radial steam turbine with a diameter of 15 mm. It has a partial admission (21%) in order to reduce the tip clearance losses, and a low reaction (15%). It is designed to operate at a 175krpm rotational speed with an inlet mass flow rate of 2.3 kgh^{-1} and a nominal total-to-total pressure ratio of 2.0. The power delivered by the turbine is on the order of 34 W and its total-to-total isentropic efficiency is estimated to be 37%.

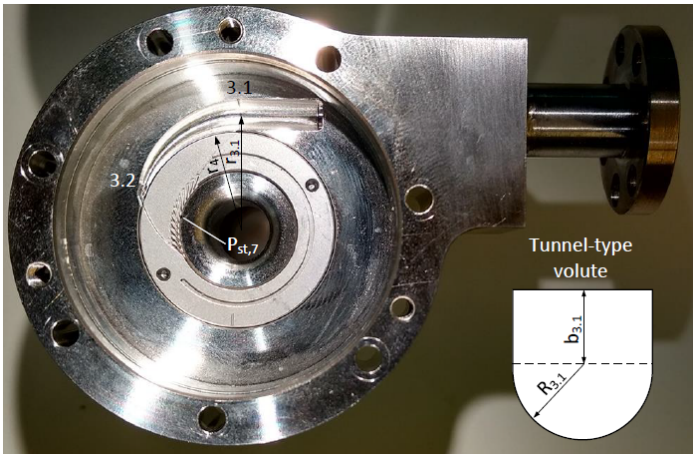

Figure 2: Small-scale radial steam turbine [1]

1.3 Objectives

The FTU was experimentally investigated. The experimental measurements done on the fan displayed reasonable correlations with the results of the numerical simulations.
However, the experimental and numerical results for the performance of the turbine, such as the total-to-total isentropic efficiency and the power, still have a potential for improvement. In fact, due to the small size of the studied unit, the torque cannot be directly measured in order to evaluate the power of the unit. The challenge is, therefore, to estimate the performance of the unit through thermodynamics laws, where heat transfer effects are not negligible.

The goal of the project is to improve the consistency as well as the quality of the results for the turbine of the FTU. Therefore, new experimental measurements were conducted on the turbine, specifically temperature and pressure measurements, targeting a refinement of the collected data. The new experimental results are furthermore implemented in the numerical model of the turbine, in order to obtain a more accurate model. Moreover, a heat investigation is done on the FTU in order to evaluate the main heat losses from the unit to the environment.

2 | Theory

This chapter introduces the main theory [2] used throughout this report, for the post-processing of the experimental, as well as the numerical data. Since it is not possible to directly deduce the power of the turbine by measuring the torque, thermodynamics laws will be used in order to determine the turbine performance parameters. The following equations are valid for a constant mass flow rate and negligible heat transfers.

2.1 Power

Using the first law of thermodynamics, the power of the turbine is given by

$$P_{turb} = \dot{m}(h_{t,in} - h_{t,out}) \tag{1}$$

where $\dot{m}$ is the constant mass flow of the turbine, $h_{t,in}$ is the total specific enthalpy at the inlet of the turbine, and $h_{t,out}$ the total specific enthalpy at the outlet of the turbine.

2.2 Total-To-Total Isentropic Efficiency

The total-to-total isentropic efficiency of the turbine

$$\eta_{turb} = \frac{P_{turb}}{P_{turb,is}} \tag{2}$$

is calculated with the turbine power from equation 1 and the isentropic turbine power

$$P_{turb,is} = \dot{m}(h_{t,in} - h_{t,is,out}) \tag{3}$$

where $h_{t,is,out}$ is the total specific enthalpy at the outlet of an isentropic turbine, i.e., the specific entropies at the turbine inlet and outlet are equal.

$$s_{in} = s_{is,out} \tag{4}$$

Given the power of the fan (P_{fan}) and the total-to-total isentropic efficiency of the fan (η_{fan}), it is possible to establish the following relations. The mechanical efficiency of the FTU

$$\eta_{mech} = \frac{P_{fan}}{P_{mech} + P_{fan}} = \frac{P_{fan}}{P_{turb}} \tag{5}$$

is calculated with the fan power (P_{fan}) and the turbine power from equation 2.The mechanical losses in the shaft and in the bearings

$$P_{mech} = P_{turb} - P_{fan} \tag{6}$$

is the difference between the turbine power and the fan power.
The overall efficiency of the FTU [3]

$$\eta_{FTU} = \eta_{turb}\eta_{fan}\eta_{mech} \tag{7}$$

$$\eta_{FTU} = \frac{P_{turb,is}}{P_{fan,is}} \tag{8}$$

can be calculated either with the components efficiencies (eq. 7) or with the turbine and fan isentropic powers (eq. 8).

2.3 Degree of Reaction

The degree of reaction of a turbine is defined as the ratio of the static-to-static enthalpy difference in the rotor (Δh_{rotor}) to the static-to-static enthalpy difference in the stage (Δh_{stage}).

$$\delta = \frac{\Delta h_{rotor}}{\Delta h_{stage}} \tag{9}$$

However, due to experimental constraints, the static temperature cannot be evaluated at the interface between the rotor and the stator, in order to determine the static specific enthalpy at this point.
The degree of reaction .

$$\delta = \frac{p_{rs} - p_{amb}}{p_{in} - p_{amb}} \tag{10}$$

is, therefore, estimated using the ratio of the static pressure : the static pressure at the rotor-stator interface (p_{rs}) ,the static inlet pressure (p_{in}) and the ambient pressure (p_{amb}).

3 | Experimental Investigation

3.1 Test and Measurement Setup

The turbine was tested experimentally with cold ambient air, as well as hot air at rotational speeds ranging from 110krpm to 175krpm. The fluid exits the turbine at ambient pressure. The setup corresponds to the one presented by Wagner et al. [1]. Additionally, new temperature and pressure measurements were conducted, in order to provide supplementary

results. For the hot air test, the fluid entered the turbine at a temperature of 220°C, while the FTU was placed inside an electric oven at 180°C.

Figure 3: Turbine test rig and sensors

Sensors During the tests, mass flow rate, temperature and static pressure measurements were conducted. The sensors used for the test rig in Figure 3 are listed in Table 1.

Table 1: Sensors used for the measurements

Measured Quantity	**Sensor**	**Measurements Characteristics**
Mass flow rate at the inlet in kgh^{-1}	*Emerson* D S006S Corilis mass flow meter (air tests)	Uncertainty of $\pm(0.002 + \frac{0.006}{\dot{m}_{in}})100\%$
Static gauge pressures in bar	*Scanivalve* DSA 3217	Uncertainty of ±0.02% Range of 6.9bar
Ambient pressure in bar	*Lufft* Opus 20	Uncertainty of ±0.5 mbar
Temperatures	Class 1 k-type thermocouples	Calibrated Uncertainty of ±0.5°C
Rotational speed in rpm	*Philtec* D20 optical probe	Sampling Rate of 50kHz Uncertainty of ±0.5krpm

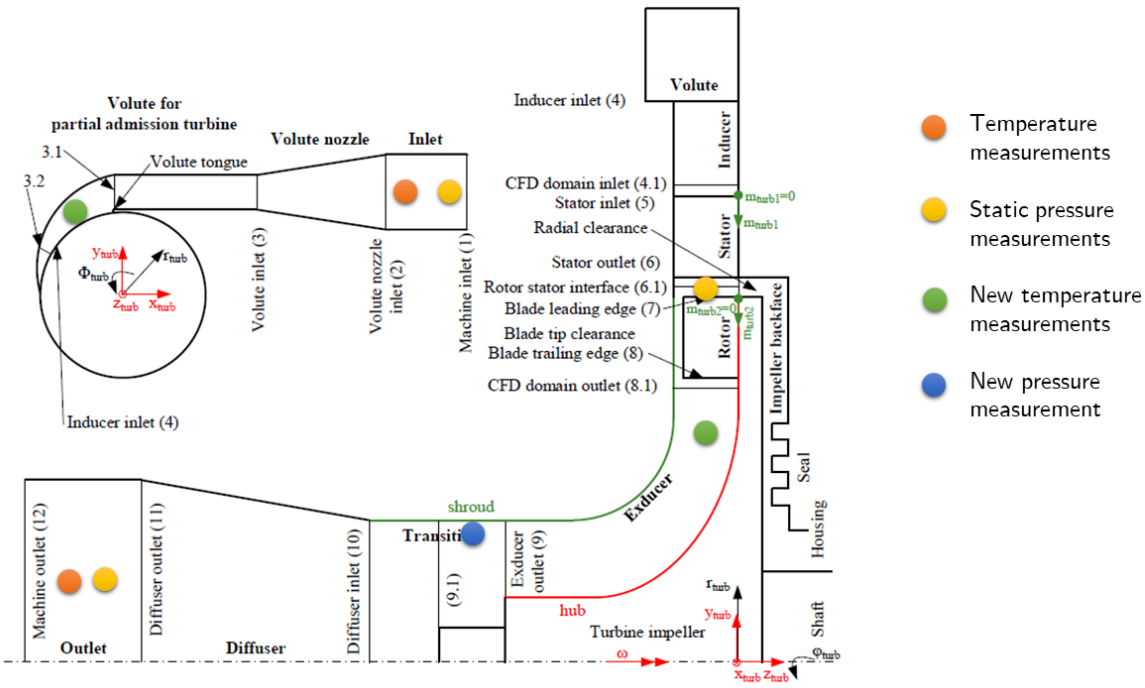

Figure 4: Temperature and pressure measurements locations (adapted from Wagner[1])

Measured quantities The mass flow rate ($\dot{m}_{in}$) was measured at the turbine inlet. The static gauge pressure was measured at the inlet (p_{in}), at the outlet (p_{out}) and at the rotor-stator interface (p_{rs}). A new pressure measurement was added at the turbine shroud (p_{shroud}).
The temperature measurements are summarised Table 2.

Table 2: Temperature measurements

Location	**Thermocouple Diameter in mm**	**Immersion Depth**
Inlet (T_{in})	⌀1.5 ⌀1.5	Wall-mounted 2 × diameter
* Volute (T_{volute})	⌀0.15	6.6 × diameter
*Downstream of the trailing edge (T_{TE})	⌀0.15	3.7 × diameter
Outlet (T_{out})	⌀1.5 ⌀1.5	2 × diameter 2 × diameter

* The volute and trailing edge temperature measurements correspond to the new temperature measurements. The new thermocouples with a diameter of 0.15mm provide more accurate measurements, however, they are less robust, more complicated to install and to seal than the thermocouples with a 1.5mm diameter (Figure 5). The holes of these two 0.15mm thermocouples were sealed using a *Loctite* EA 9497 glue, which is resistant up to a 180°C temperature.

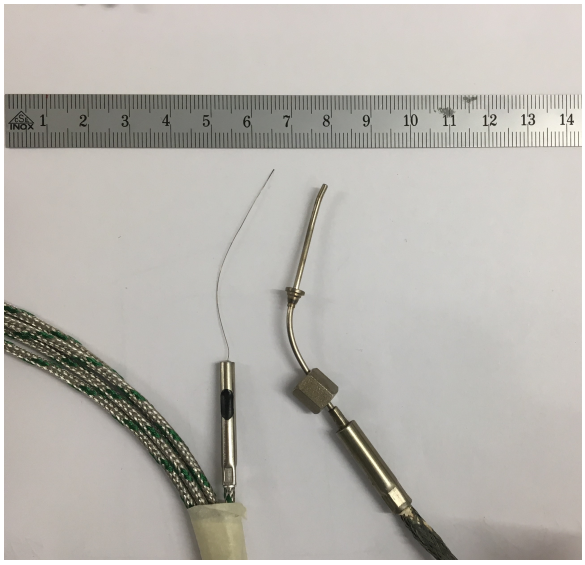

Figure 5: k-Type thermocouples with a diameter of 0.15mm (left) and 1.5mm (right)

Since heat transfers occur between the working fluid and the environment, the temperature measurements are affected by heat transfers. As seen on Figure 4, the temperature measured at the turbine volute and the trailing edge are closer to the stator and the rotor. Therefore, the impact of the heat transfer should be reduced on the new measurements and, using the equations presented in Section 2, the performance of the turbine would be evaluated with more accuracy.

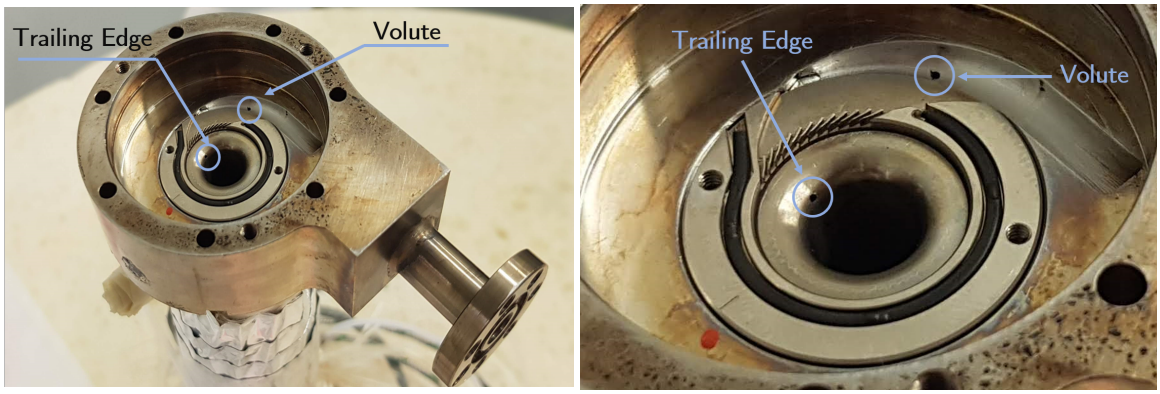

Figure 6: Position of the two new thermocouples at the volute and downstream of the trailing edge

(a) Volute (b) Downstream of the trailing edge

Figure 7: Microscope pictures of the new thermocouples at the volute (a) and downstream of the trailing edge (b)

3.2 Temperature Measurements

The velocity of the working fluid in the turbine can go up to a Mach number of $M = 1$. Due to the viscous dissipation of the fluid and heat losses by conductivity, the kinetic energy of the fluid is not entirely converted to thermal energy at the surface of the thermocouple. This means that the measurement of the thermocouple is between the static temperature and the total temperature [4]. The recovery factors of the thermocouples are thus taken into account as shown in Appendix A for the measurements at the inlet, at the volute, downstream of the trailing edge, and at the outlet to accurately determine these total temperatures.

3.2.1 Cold Air Test

The air enters the turbine at ambient temperature, around $24°C$. The measurements were conducted in steady-state conditions with multiple rotational speeds between 120krpm and

175krpm. The collected temperature measurements with their respective rotational speeds are reported in Figure 8 with respect to the total-to-total pressure ratio.

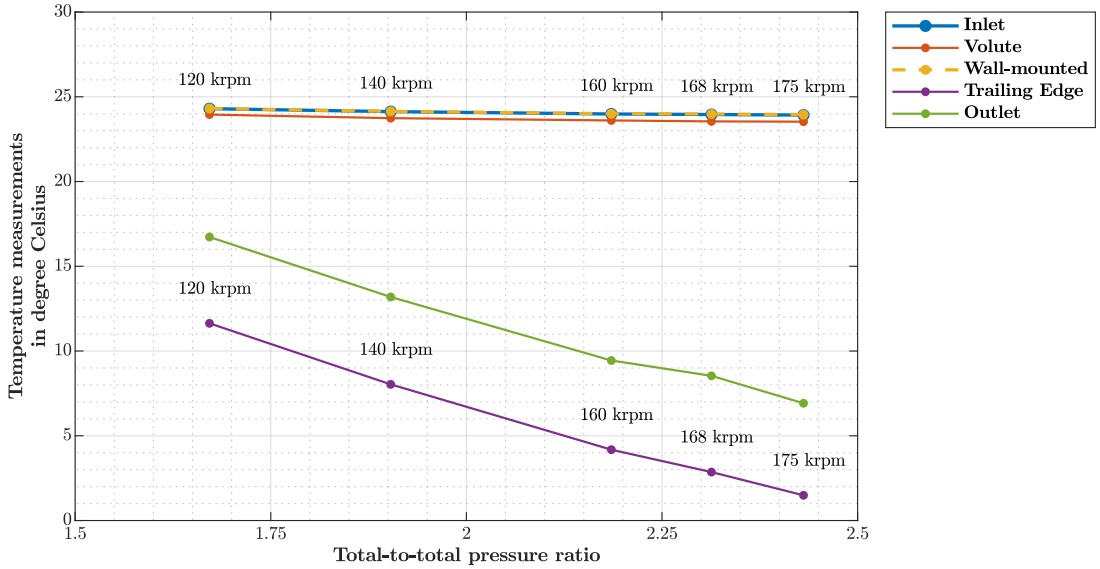

Figure 8: Temperature measurements for the cold air test at different rotational speeds with respect to the total-to-total pressure ratio

Inlet of the turbine The air enters the turbine at ambient temperature. Hence, negligible heat transfer occurs between the fluid and the environment. The three thermocouples at the inlet,i.e., Inlet, Volute and Wall-mounted in Figure 8 indicate approximately the same temperature.

Outlet of the turbine At the outlet of the turbine, the air exits with a temperature which is lower than the ambient temperature. This temperature difference induces heat transfers from the environment of the turbine to the working fluid. As seen in Figure 8, the temperature will rise between the trailing edge and the outlet measurements by about $5°C$. Assuming a constant specific heat capacity $c_p = 1.006$kJ kg^{-1}K^{-1} and a constant mass flow rate, the heat transferred is approximated as

$$Q = \dot{m} c_p (T_{out} - T_{TE}) \tag{11}$$

resulting in heat transfers increasing from 4.2W at 120krpm to 7.4W at 175krpm.

Furthermore, the outlet temperatures follow the same trend,i.e., they decrease as the rotational speed increases. The temperature downstream of the trailing edge decreases from $11.6°C$ to $1.5°C$ with the increase of the total-to-total pressure ratio. In fact, the higher are the rotational speed and the total-to-total pressure ratio, the more energy will be extracted from the fluid and converted into mechanical work.

3.2.2 Hot Air Test

The air was heated until a temperature of 220°C using an evaporator before entering the turbine. The measurements were conducted in steady-state conditions at different rotational speeds ranging from 110krpm to 175krpm. The FTU was placed in an electrical oven at 180°C. The different temperature measurements presented in Table 2 are displayed in Figure 9.

The ambient temperature corresponds to the oven temperature. The temperature of the working fluid is higher than the ambient temperature, inducing heat transfers from the fluid to the environment.

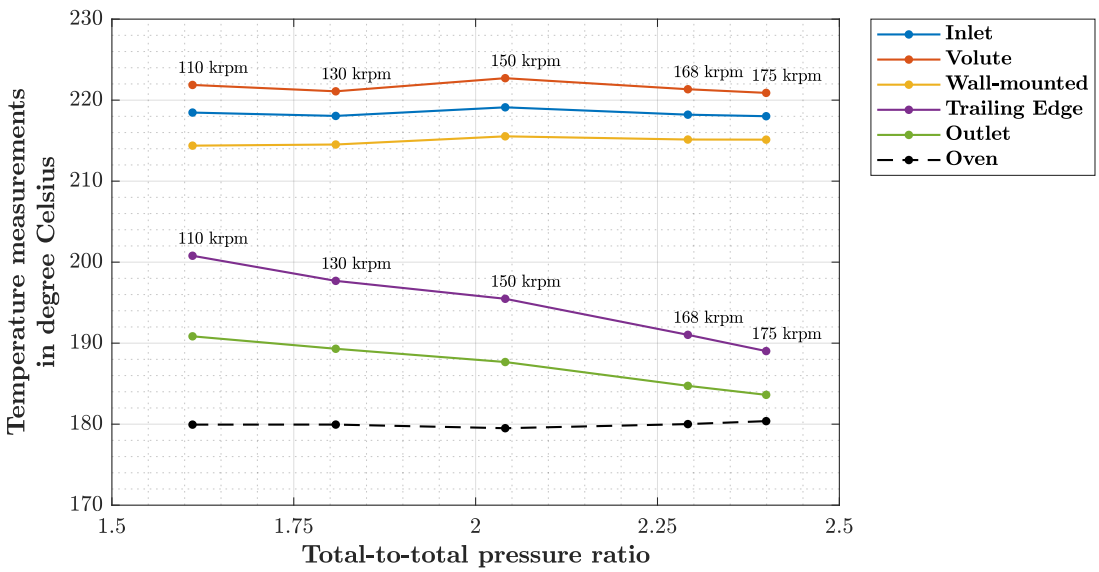

Figure 9: Temperature measurements for the hot air test at different rotational speeds with respect to the total-to-total pressure ratio

Inlet of the turbine Due to heat transfers, the temperature at the turbine inlet is expected to decrease from the inlet thermocouple to the volute thermocouple. However, the volute temperature is unexpectedly the highest. This could be explained by the immersion depth of the thermocouples. According to Liptak [5], as well as *Conax Technologies* [6], the immersion depth for the thermocouple should be ideally larger than ten times the diameter, in order to limit the impact of the heat conduction through the thermocouple on the measurements. At the inlet, one thermocouple is wall-mounted (yellow line in Figure 9), one is immersed two times its diameter due to dimension constraints (blue line in Figure 9), and the one at the volute has an immersion depth of 6.6 times the diameter (orange line in Figure 9), hence, the volute measurements are the most accurate. Nevertheless, the temperature measurements at the inlet correlate within 3.4°C and follow the same trend.

Outlet of the turbine At the outlet of the turbine, the difference in the measurements at the outlet and the trailing edge is significant, ranging from 5°C to 10°C . At the trailing

edge, the temperature is above the oven temperature. Due to heat fluxes to the environment, the temperature decreases and, therefore, the temperature measured at the outlet is lower. Moreover, the turbine outlet temperatures are above the oven temperature. They decrease with increasing rotational speed, and thus increasing total-to-total pressure ratio, i.e., the trailing edge temperature decreases from 200.8°C (pressure ratio of 1.6) to 189°C (pressure ratio of 2.3).

3.3 Methodology

In order to determine the performance parameters of the turbine, the equations presented in Section 2 are used. The required thermodynamics properties (specific enthalpy and entropy) are evaluated using the temperature and pressure measurements with a fluid database (REFPROP[7]). It is assumed that there is no leakage,i.e., the mass flow rate is constant. The degree of reaction is given by equation 10.

Power The powers are derived from equation 1.

$$P_{turb,old} = \dot{m}_{in}(h(T_{in}, p_{t,in}) - h(T_{out}, p_{amb})) \tag{12}$$

$$P_{turb,new} = \dot{m}_{in}(h(T_{volute}, p_{t,volute}) - h(T_{TE}, p_{amb})) \tag{13}$$

Isentropic Power The isentropic powers are determined using equation 3.

$$P_{turb,is,old} = \dot{m}_{in}(h(T_{in}, p_{t,in}) - h(s(T_{in}, p_{t,in}), p_{amb})) \tag{14}$$

$$P_{turb,is,new} = \dot{m}_{in}(h(T_{volute}, p_{t,volute}) - h(s(T_{volute}, p_{t,volute}), p_{amb})) \tag{15}$$

Isentropic Total-to-Total Efficiency From equation 2 the isentropic total-to-total efficiency is computed as follows.

$$\eta_{turb,old} = \frac{h(T_{in}, p_{t,in}) - h(T_{out}, p_{amb})}{h(T_{in}, p_{t,in}) - h(s(T_{in}, p_{t,in}), p_{amb})} \tag{16}$$

$$\eta_{turb,is,new} = \frac{h(T_{volute}, p_{t,volute}) - h(T_{TE}, p_{amb})}{h(T_{volute}, p_{t,volute}) - h(s(T_{volute}, p_{t,volute}), p_{amb})} \tag{17}$$

It is important to note that the total pressure at the volute takes into account the pressure loss between the inlet and the volute of the turbine.

$$p_{t,volute} = p_{t,in} - p_{loss} \tag{18}$$

p_{loss} is the pressure loss computed following the method presented by Font [8]. The maximum pressure loss is of 15.2 mbar.

Corrected Isentropic Total-to-Total Efficiency Is it also possible to evaluate the isentropic total-to-total efficiency from equations 5, 7 and 8.

$$\eta_{FTU} = \frac{P_{fan,is}}{P_{turb,is}} \tag{19}$$

$$\eta_{turb,corr} = \frac{\eta_{FTU}}{\eta_{fan}\eta_{mech}} \tag{20}$$

In this case, the result does not depend on the outlet temperatures of the working fluids of the fan and the turbine. Thus, this measurement is suggested to be less influenced by heat conduction effects.

Corrected Power Furthermore, using the corrected isentropic total-to-total efficiency (eq. 20), and the turbine isentropic power (eq. 15) the power of the turbine is computed.

$$P_{turb,corr} = \eta_{turb,corr} P_{turb,is,new} \tag{21}$$

4 | Numerical Investigation

4.1 Numerical Setup

The CFD simulation is carried out with the commercial software *Ansys* CFX 19.2. A mesh sensitivity analysis was conducted (Appendix B). A mesh formed with 0.6m nodes is selected in order to insure the convergence of the results and an average y^+ value close to 1.

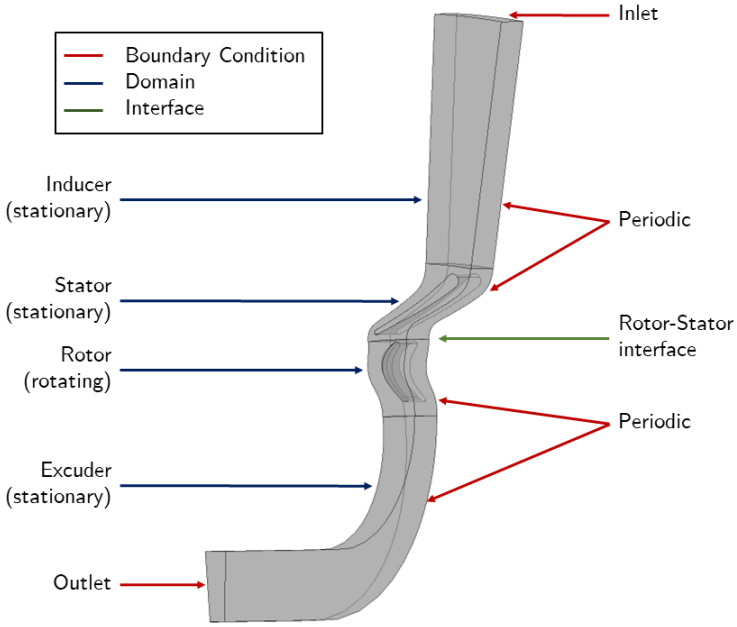

Figure 10: CFD numerical model of a single-passage of the turbine

For the ambient and hot air simulations, a compressible and non-isothermal ideal gas model

is selected. Moreover, at the inlet boundary condition, the SST turbulence model with a medium turbulence intensity of 5% is taken into account. The stator has $n_{stator} = 12$ blades and the rotor has $n_{rotor} = 59$ blades.

The simulation consists of a steady single-passage with periodic boundary conditions, as seen in Figure 10. This implies that some of the losses due to the partial admission, such as the empty-filling losses at the start and the end of the admission, respectively, as well as the pumping effect of the non-admission turbine blades are not taken into consideration. Therefore, the CFD model is expected to overestimate the power and the efficiency of the turbine.

4.2 Boundary Conditions

The boundary conditions selected for the simulation are the rotational speed, the total temperature and the total pressure at the inlet, and the static pressure at the outlet. The new measurements are taken into account for the boundary conditions of the simulations.

- The rotational speed corresponds to the measured rotational speed Ω.
- The total pressure at the inlet corresponds to the total pressure at the volute ($p_{t,volute}$) given by equation (18), computed by taking into consideration the pressure loss at the inlet.
- The total temperature at the inlet is given by the total temperature measured at the volute (T_{volute}).
- The static pressure at the outlet is the static pressure measured at the shroud (p_{shroud}).

4.3 Method

The simulation is used to compute numerically the mass flow rate in the turbine,the power, the total-to-total isentropic efficiency, and the degree of reaction. These quantities will be compared afterwards to the experimental results.

Power The one-passage turbine power is given by the torque of the impeller and the excuder hub around the rotational axis multiplied with the angular velocity of the turbine.

Since it is a one-passage simulation, the total mass flow rate $\dot{m}_{in,CFD}$ and power $P_{turb,CFD}$ are determined by multiplying the one-passage value by a factor of $n_{rotor} + 1 = 13$.

Isentropic total-to-total efficiency The isentropic total-to-total efficiency is evaluated as the ratio of the specific enthalpy drop in the turbine to the specific enthalpy drop for an isentropic turbine computed using equation 15.

$$\eta_{turb,CFD} = \frac{P_{turb,CFD}/\dot{m}_{in,CFD}}{P_{turb,is,new}/\dot{m}_{in}} \tag{22}$$

Degree of Reaction To evaluate the degree of reaction, the static pressure at the rotor-stator interface is determined numerically. It corresponds to the line-averaged pressure at the shroud at the rotor-stator interface. The degree of reaction is then computed using equation 10 with the experimental inlet static pressure (p_{in}) and ambient pressure (p_{amb}).

5 | Analytical Investigation

An analytical investigation was conducted on the turbine using a one-dimensional model, in order to estimate the isentropic total-to-static efficiency. The result depends on the turbine rotational speed, and on several turbine geometrical parameters [3] :

- Absolute blade angle at the rotor leading edge based on the circumference $\alpha_{LE} = 22°$
- Absolute blade angle at the rotor trailing edge based on the circumference $\beta_{TE} = 41.7°$
- Radius at the rotor leading edge $r_{LE} = 7.50mm$
- Radius at the rotor trailing edge $r_{TE} = 6.50mm$
- Rotor blade height $H = 0.586mm$

Soderberg [9] describes a loss correlation for turbines at optimal load coefficient according to the Zweifel criterion [10] at zero incidence, a Reynolds number based on the hydraulic diameter of the throat section, an aspect ratio defined with the blade height and the radial blade chord, a maximum blade thickness to radial chord ratio ($\frac{t_{max}}{r_{LE}-r_{TE}}$) of 0.2, and a deflection lower than 120°.

The Reynolds number is based on the hydraulic diameter (d_{hyd}) corresponding to the throat section at the rotor trailing edge. It is defined with the channel depth ($\frac{\pi d_{TE}}{n_{rotor}} \cos \beta_{TE,blade}$) and the rotor blade height (H).

$$d_{hyd} = \frac{2\frac{\pi d_{TE}}{n_{rotor}} \cos \beta_{TE,blade} H}{\frac{\pi d_{TE}}{n_{rotor}} \cos \beta_{TE,blade} + H} \tag{23}$$

The aspect ratio

$$\frac{H}{r_{LE} - r_{TE}} \tag{24}$$

depends on the blade height (H) and the radial blade chord ($r_{LE} - r_{TE}$).

The "nominal" loss coefficient, defined for a Reynolds number of 10^5 and an aspect ratio of 3

$$\zeta = 0.04 + 0.06 \left(\frac{\frac{\pi}{2} - \alpha_{LE} + \frac{\pi}{2} - \alpha_{TE}}{\pi \frac{100}{180}} \right)^2 \tag{25}$$

is a function of the blade deflection.

Otherwise, if the Reynolds number or the aspect ratio do not verify the conditions above, the nominal loss coefficient is adapted for the rotor and the rotor using the correlations 26 and 27 provided by Soderberg [9].

$$\zeta_{stator} = 1 - (1 + \boldsymbol{\zeta}) \left(0.993 + 0.021 \frac{r_{LE} - r_{TE}}{H} \right) \left(\frac{10^5}{Re_{d_{hyd}}} \right)^{0.25} \tag{26}$$

$$\zeta_{rotor} = 1 - (1 + \boldsymbol{\zeta}) \left(0.975 + 0.075 \frac{r_{LE} - r_{TE}}{H} \right) \left(\frac{10^5}{Re_{d_{hyd}}} \right)^{0.25} \tag{27}$$

The total-to-static isentropic efficiency is thus a function of the loss coefficients adapted for the rotor (eq. 26) and the stator (eq. 27), as well as the turbine total-to-total specific enthalpy difference (Δh_{tt}).

$$\eta_{is,tst} = \frac{1}{1 + \frac{1}{2\Delta h_{tt}} \left(\zeta_{rotor}\omega_{TE}^2 + \zeta_{stator}c_{LE}^2 + c_{TE}^2\right)} \tag{28}$$

The total-to-static isentropic efficiency is evaluated based on the mean-line analysis and following an iterative process to determine the input parameters ($Re_{d_{hyd}}$, Δh_{tt}, ω_{TE}, c_{LE}, and c_{TE}).

6 | Results & Discussion

The performance results for both the cold air and the hot air tests conducted on the turbine are summarised in the following Figures 11 and 12 respectively. The various procedures used to evaluate the turbine parameters are compared.

6.1 Cold Air Test

It is important to note that the cold air test is carried out without the fan volute, hence, it is not possible to compute the corrected power and isentropic total-to-total efficiency with the available data (according to equations 20 and 21). It should also be noted that the maximum uncertainties on the experimental mass flow rate, total-to-total pressure ratio, and degree of reaction are 0.0153kgh^{-1}, 0.0015 and 0.036%, respectively, which are negligible and are therefore not represented on Figure 11.

Mass flow rate It is assumed that there is no leakage in the turbine, and the inlet mass flow rate remains constant. The first graph in Figure 11 compares the experimentally measured and numerically computed mass flow rates. As expected, in both cases, the mass flow rate increases as the total-to-total pressure ratio and the rotational speed increase. However, the CFD mass flow rate underestimates the mass flow rate by 16% . The mass flow at the inlet increases from 2.9kgh^{-1} to 4.6kgh^{-1} as the total-to-total pressure ratio is higher.

Power The power increases with the total-to-total pressure ratio and the rotational speed. The power determined with the new measurements (eq. 13) is higher than the power evaluated with the old measurements (eq. 12). In fact, with the new measurements, the temperature difference between the inlet and outlet is larger, and, therefore, represents a higher power extracted from the working fluid. The new measurements results are in better agreement with the CFD results, which still overestimate the power by 20% at 175krpm. The new measurements refine the results by reducing the impact of the heat transfer from the ambient environment ($24°C$) to the fluid, which is at a lower temperature. The new results, therefore, display improvements. The power reaches a value of 28W at the design speed of 175krpm while evaluated with the new measurements (eq. 13).

Isentropic total-to-total efficiency The new experimental total-to-total isentropic efficiency (eq. 17) is higher than the initial experimental value (eq. 16), and closer to the

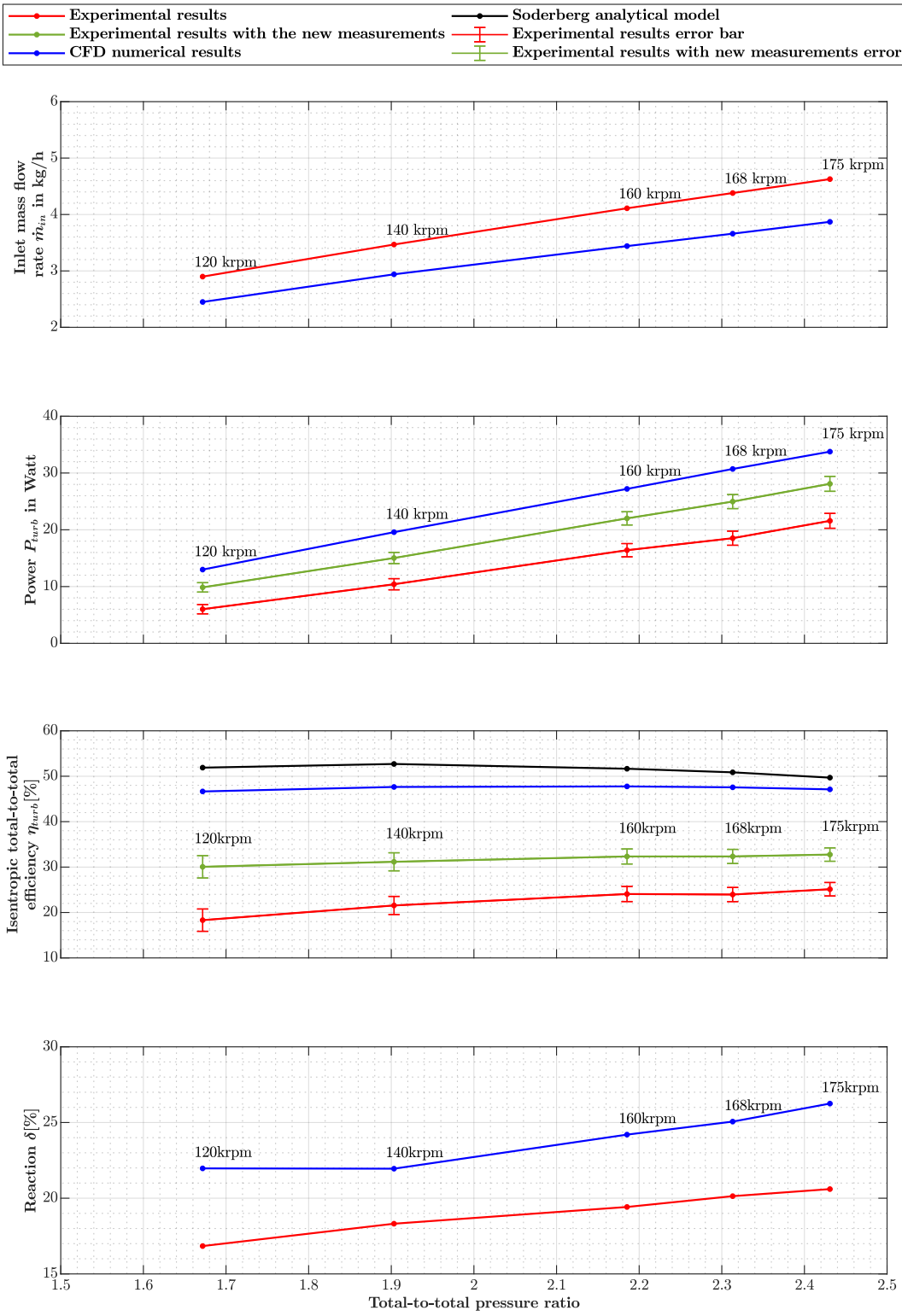

Figure 11: Performance results of the cold air test conducted on the turbine

numerical result (eq. 22). However, the numerical results still overestimate the isentropic total-to-total efficiency by more than 40% for the reasons presented in Section 4.1.
As for the Soderberg analytical model, it should be used under the assumption that the turbine is operated at the design point. However, in this case, the turbine is operated with ambient air, while it is designed to operate with steam entering at a temperature of $220°C$. Therefore, the Soderberg model is not accurate for these tests. This explains the large difference between the analytical and the experimental results.
At the design rotational speed (175krpm), the new experimental efficiency is around 32%, whereas the initial experimental efficiency displays values on the order of 24%. Following the same reasoning as for the power and considering that the influence of heat transfers on the results are limited with the new measurements, an isentropic total-to-total efficiency of 32% would be a better approximation of the actual efficiency.

Degree of Reaction The degrees of reaction determined experimentally (eq. 10) and numerically follow the same trend between rotational speeds of 140krpm and 175krpm. The experimental degree of reaction increases with the total-to-total pressure ratio up to a value of 20.6% at the design rotational speed (175krpm). The CFD result is higher than the experimental result by around 25%. In fact, for each case rotational speed, the numerically computed static pressure at the rotor-stator interface is higher than the experimental value, leading to a higher degree of reaction. The rotor-stator interface presents transient effects which are not captured by a steady-state numerical simulation, thus explaining the significant difference between the results.

6.2 Hot Air Test

The maximum uncertainties on the experimental mass flow rate, total-to-total pressure ratio, and degree of reaction are 0.0131kgh^{-1}, 0.0014 and 0.038%, respectively.They are, therefore, neglected and not represented on Figure 12.

Inlet mass flow rate The inlet mass flow rate increases from 2.1 kgh^{-1} to 3.5kgh^{-1} as the total-to-total pressure ratio increases. The CFD mass flow rate underestimates the real mass flow rate by 20%.

Power The power evaluated experimentally, numerically, and the corrected power follow the same trend, they increase as the rotational speed and the total-to-total pressure ratio of the turbine increase.
First, the power evaluated experimentally with the initial measurements (eq. 12) is higher than the power determined with the new measurements (eq. 13). In fact, as seen in Section 3.2.2, the temperature measured at the trailing edge is higher than the temperature measured at the outlet, while the inlet and volute temperature measurements are close. This is due to heat transferred from the working fluid at the turbine outlet to the oven which is at a lower temperature. Moreover, as the total-to-total pressure ratio increases, the powers evaluated experimentally are in better agreement reaching a 7.85% relative difference at 175krpm. In fact, when the total-to-total pressure ratio increases, the difference between the trailing edge and the outlet temperatures decreases, and both temperature are closer to the oven temperature, leading to less heat transfers. The new experimental power at the design rotational speed (175krpm) is 32W.

The numerical power is higher and increases faster than the experimental powers resulting in a relative difference of 22.85% between the new experimental measurements and the numerical model power at 175krpm.
The corrected power (eq. 21) corresponds to the highest value (46.5W at 175krpm). In fact, equation 6 assumes that the fan and the turbine are perfectly insulated from the heat dissipated by the mechanical losses. However, the mechanical losses have a contribution on the measured powers (see Section 7), thus, defining the power of the turbine as in equation 6 overestimates the actual value.

Isentropic total-to-total efficiency The trends followed by the different models vary. First, as the total-to-total pressure ratio increases, the new experimental efficiency (eq. 17) and the initial experimental efficiency (eq. 16) both decrease due to important heat transfers from the air to the oven at the turbine outlet. Moreover, they are in better agreements for high rotational speeds, with a relative difference of 8.49% at 175krpm. In fact, when the rotational speed increases, the heat transfers at the turbine outlet are lower. The isentropic total-to-total efficiency evaluated experimentally with the new measurements is 29.63% at 175krpm.
The numerical (eq. 22) and corrected efficiencies (eq. 20) increase with the total-to-total pressure ratio, reaching 45.25% and 43.07%, respectively, at 175krpm. Moreover, they overestimate the actual efficiency of the turbine.
The Soderberg analytical model efficiency (eq. 28) is somewhat a "compromise" between the efficiencies of the other models and seems to be a good approximation of the actual efficiency of the turbine at the design operating speed of 175krpm with a value of 39.5%.

Degree of Reaction The degrees of reaction determined experimentally (eq. 10) and numerically follow the same trend. They increase with the total-to-total pressure ratio reaching a value of 16.1% at the design rotational speed. The CFD result overestimates the experimental result by more than 25% for the same reasons presented in Section 6.1.

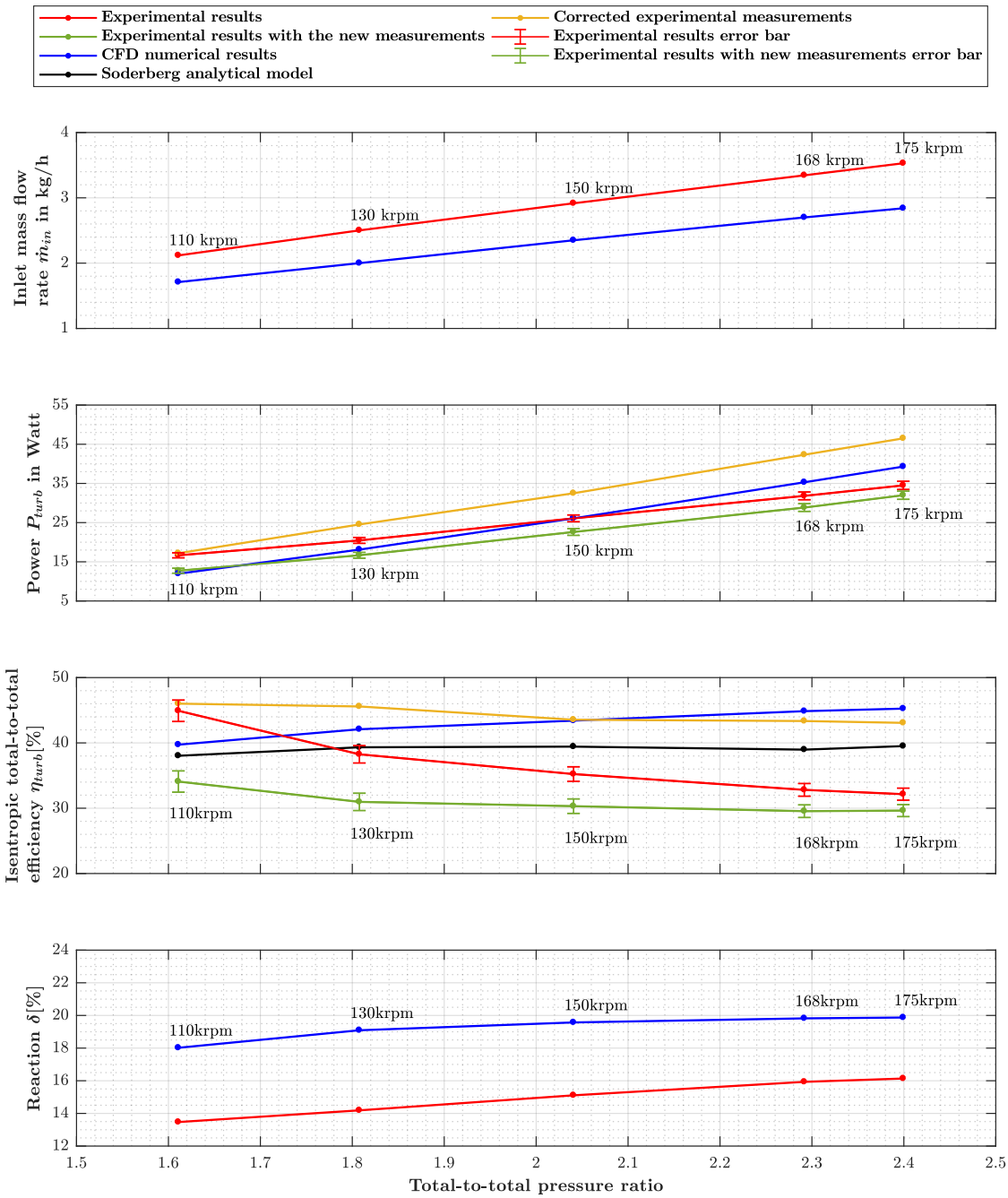

Figure 12: Performance results of the hot air test conducted on the turbine

7 | Heat Investigation

In the case of the hot air test, important heat transfers occur, due to temperature differences between the working fluid and the oven throughout the FTU, as well as heat dissipation due to the mechanical losses. The goal of this section is to approximate the heat losses to the environment using a simplified heat transfer model of the FTU.

7.1 FTU Heat Losses

The heat losses to the environment are first studied in the case of the overall FTU, and then by focusing on the turbine only.

7.1.1 Methodology

The dissipated heat is due to the mechanical losses at the shaft. This heat is exchanged throughout the FTU and with the environment. The following equation displays the relation between the power of the turbine, the power of the fan and the mechanical losses.

$$P_{turb,real} = P_{fan,real} + P_{mech} \tag{29}$$

However, in the case of the hot air test, the temperatures of the working fluids of the fan and the turbine vary within a wide range which is different from the oven temperature, generating heat transfers within the system, as well as heat losses to the environment Q_{loss}.

The remaining dissipated heat which is not transferred to the environment ($P_{mech} - Q_{loss}$) is transferred to the turbine and to the fan, impacting the experimental evaluation of the power.

In the ideal case, the components of the FTU would be perfectly insulated from each other and from the surroundings. This means that the turbine and the fan would be adiabatic and there would not be any heat fluxes to and/or from this components, the heat dissipated would only be exchanged with the environment. Since the fan and and turbine inlet temperatures are fixed, in the absence of heat transfers to these components, the ideal outlet temperatures of the turbine and the fan would be lower than the measured temperatures. This implies that the turbine power evaluated experimentally (P_{turb}) is an underestimation of the actual turbine power ($P_{turb,real}$), whereas the fan power evaluated experimentally (P_{fan}) is an overestimation of the actual fan power ($P_{fan,power}$).

If it is assumed that a fraction x of the dissipated heat is exchanged with the turbine and the remaining $(1 - x)$ is exchanged with the fan, the following relations between the actual and the experimental powers are established.

$$P_{turb,real} = P_{turb} + x(P_{mech} - Q_{loss}) \tag{30}$$

$$P_{fan,real} = P_{fan} - (1 - x)(P_{mech} - Q_{loss}) \tag{31}$$

By replacing equations 30 and 31 in equation 29, it is possible to compute experimentally the heat losses transferred to the oven.

$$Q_{loss} = P_{turb} - P_{fan} \tag{32}$$

7.1.2 FTU Model

The FTU is modelled as shown in Figure 13. It is divided into five different parts : the fan-shaft-turbine cylinder, the turbine inlet, the turbine outlet, the fan inlet, and the fan outlet. Each component is studied independently and presents the heat transfer mechanisms displayed in Figure 13. All the components are made of steel with a heat conductivity of $k_{steel} = 16\text{Wm}^{-1}\text{K}^{-1}$ [11]. The turbine and fan outlets have ten layers of glass fiber tape, each with a thickness of 0.5mm, and a thermal conductivity of $k_f = 0.5\text{Wm}^{-1}\text{K}^{-1}$. However, it is important to note that the layers of glass fiber tape are separated by layers of air which are not taken into account in the model, leading to an overestimation of the heat losses. The convective heat transfers are computed using empirical correlations from Incorpera et al. [12] under the assumptions detailed below.

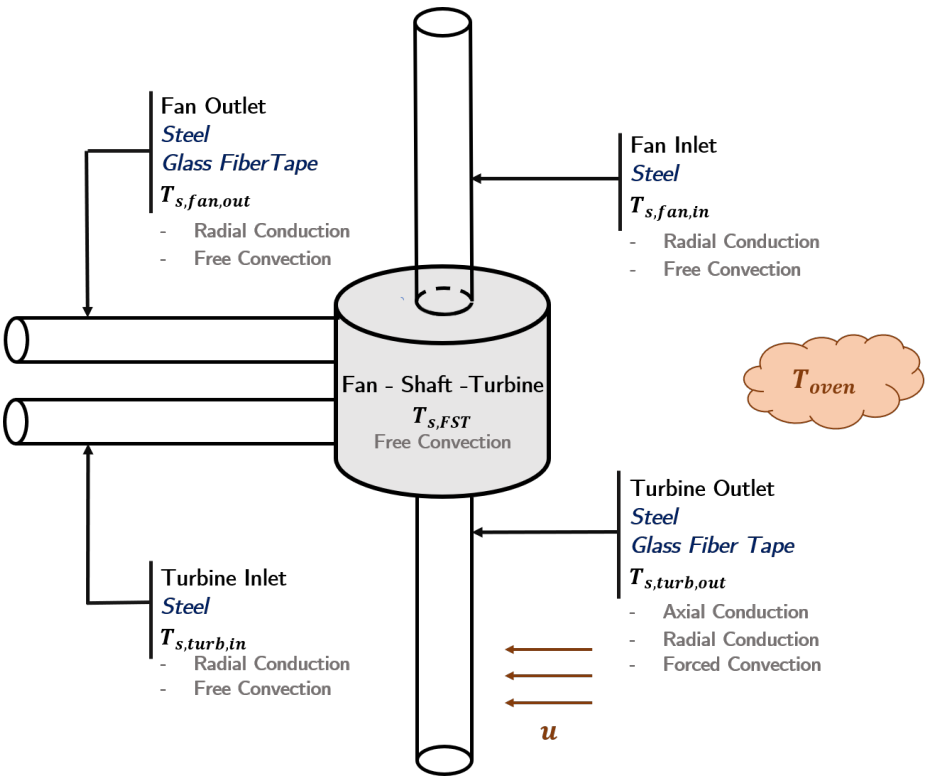

Figure 13: FTU simplified model for the heat transfer investigation

Axial heat transfer The axial heat transfer is computed at the outlet of the turbine. The total axial thermal resistance corresponds to the conduction thermal resistances of air, steel, and glass fiber tape arranged in parallel. It is important to note that the axial heat transfer is not computed at the turbine inlet because the temperature is increasing between

the inlet and the volute instead of decreasing due to heat transfers to the environment as stated in Section 3.2.2.

$$R_{ax,i} = \frac{L}{k_i A_i} \tag{33}$$

$$R_{ax,tot} = \left(\frac{1}{R_{ax,air}} + \frac{1}{R_{ax,steel}} + \frac{1}{R_{ax,f}}\right)^{-1} \tag{34}$$

$$Q_{ax} = \frac{\Delta T}{R_{ax,tot}} \tag{35}$$

Radial heat transfer The total radial thermal resistance corresponds to the thermal resistance of conduction in steel and glass fiber tape computed as in equation 36, and the thermal resistance of convection given by equation 37 arranged in series.

$$R_{rad,i} = \frac{ln(r_{i,2}/r_{i,1})}{2\pi L k_i} \tag{36}$$

$$R_{conv} = \frac{1}{2\pi r L h} \tag{37}$$

$$R_{rad,tot} = R_{rad,steel} + R_{rad,f} + R_{conv} \tag{38}$$

$$Q_{rad} = \frac{\Delta T}{R_{rad,tot}} \tag{39}$$

The convective heat transfer is either natural or forced, the properties of the fluid required in the correlations are determined at the film temperature of the fluid $T_f = \frac{T_s + T_{oven}}{2}$. In the case of the fan-shaft-turbine cylinder, only the free convection is considered. The Nusselt number is computed in each case in order to evaluate the heat transfer coefficient.

$$h = \frac{\overline{Nu}_y y}{k} \qquad y = \{D; L\} \tag{40}$$

The Reynolds number and the Rayleigh number are used in the following correlations [12].

$$Re_D = \frac{\rho u D}{\mu} \tag{41}$$

$$Ra_y = g\beta_f \frac{\Delta T}{\nu \alpha_f} y^3 \qquad y = \{D; L\} \tag{42}$$

- The turbine inlet and the fan outlet are approximated as infinite cylinders subject to free convection. The surface temperatures are approximated as $T_{s,turb,in} = \frac{T_{in} + T_{volute}}{2}$ and $T_{s,fan,out} = T_{fan,out}$. The Nusselt number is computed in order to evaluate the heat transfer coefficient.

$$\overline{Nu}_D = \left[0.6 + \frac{0.387 Ra_D^{1/6}}{[1 + (0.559/Pr)^{9/16}]^{8/27}}\right]^2 \tag{43}$$

- The fan inlet, as well as the fan-shaft-turbine components are vertical cylinders subject

to free convection. They are therefore approximated as vertical plates subject to free convection. The surface temperatures are estimated as $T_{s,fan,in} = T_{fan,in}$ and $T_{s,FST} = \frac{T_{volute}+T_{TE}+T_{fan,in}+T_{fan,out}}{4}$.

$$\overline{Nu}_L = \left[0.825 + \frac{0.387 Ra_L^{1/6}}{[1+(0.492/Pr)^{9/16}]^{8/27}}\right]^2 \tag{44}$$

- The turbine outlet is subject to forced convection. In fact, air is flowing into the oven vertically near the turbine outlet with an estimated speed of $u = 1.5m/s$. Therefore, the turbine outlet is considered to be a cylinder in a crossflow with a surface temperature of $T_{s,turb,out} = \frac{T_{TE}+T_{out}}{2}$.

$$\overline{Nu}_D = 0.3 + \frac{0.62 Re_D^{1/2} Pr^{1/3}}{[1+(\frac{0.4}{Pr})^{2/3}]^{1/4}}\left[1+(\frac{Re_D}{282000})^{5/8}\right]^{4/5} \tag{45}$$

7.1.3 Results & Discussion

The experimental heat losses and the various heat losses computed using the model introduced previously are compared in Figure 14. The turbine and the fan heat losses correspond to the sum of the heat losses at the inlet and the outlet.

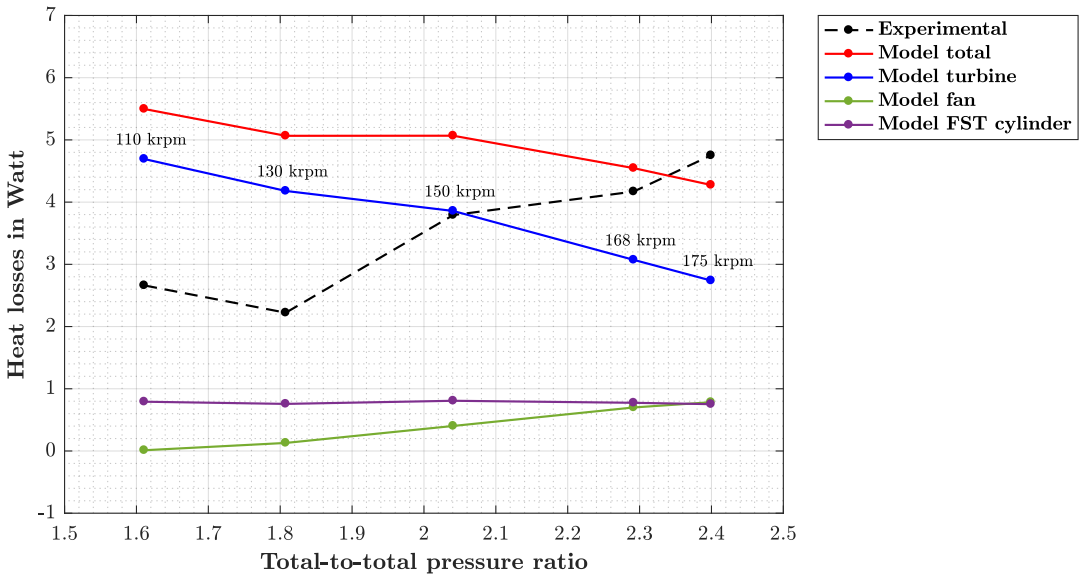

Figure 14: Heat losses determined experimentally and computed using the model with respect to the total-to-total pressure ratio

The experimental and modelled heat losses do not follow the same trend. The experimental heat losses display an increasing tendency with the total-to-total pressure ratio, whereas the heat losses computed with the simplified model are decreasing. This can be explained by the distribution of the heat losses. In fact, the turbine heat losses represent more than 60%

of the total modelled heat losses, and thus, the main source of the losses. Furthermore, as the total-to-total pressure ratio increases, the turbine losses decrease. This will be detailed in Section 7.2. On the other hand, the fan heat losses are low, ranging between 0.01W and 0.78W, and the heat losses of the fan-shaft-cylinder are constant around 0.77W within 0.02W.

It is important to note that the measured temperature at the fan inlet is 175°C ± 2°C and is thus below the oven temperature. This leads to a heat exchange from the environment to the working fluid. For low rotational speeds, the heat exchanged at the fan outlet balances the heat exchanged at the fan inlet which explains the fan heat loss at 110krpm which is close to zero (0.01W).

7.2 Turbine Heat Losses

The turbine heat losses represent the main heat losses of the FTU. A preliminary approach is thus to undertake a heat investigation focused on the turbine.

7.2.1 Methodology

Comparing the initial and the new experimental powers allows to determine the heat losses at the turbine outlet side. In fact, the new power obtained with the new measurements, which are closer to the stator and the rotor, exclude the heat losses at the outlet of the turbine. Therefore the heat losses at the turbine outlet are approximated by the difference between the experimental powers (eq. 46).

$$Q_{turb,exp} = P_{turb,old} - P_{turb,new} \tag{46}$$

However, at the turbine inlet and volute the measured temperatures are close. Moreover, the temperature increases between the inlet and the volute instead of decreasing due to the heat transfer to the environment, thus, the losses at the turbine inlet cannot be evaluated using this approach.
The total heat losses at the turbine correspond to the sum of the losses at the inlet and the outlet of the turbine computed using the previous model.

7.2.2 Results & Discussion

The total turbine heat losses as well as their different contributions are reported in Figure 15.
First of all, the modelled turbine losses decrease with the total-to-total pressure ratio until 2.74W at 175krpm. The temperature at the turbine inlet is more or less constant, generating a constant heat exchange of 1.40W±0.2W with the oven independently of the total-to-total pressure ratio.
On the other hand, the outlet heat losses represent 50% to 70% of the total turbine heat losses computed using the model. The outlet heat losses determined with the simplified model, as well as the experimental heat losses at the outlet side decrease when the total-to-total pressure ratio increase as expected. In fact, as explained in Section 3.2.2, the temperatures get closer to the oven temperature as the total-to-total pressure ratio increases, reducing the heat exchanged with the oven. This behaviour is well displayed by the model. Furthermore,

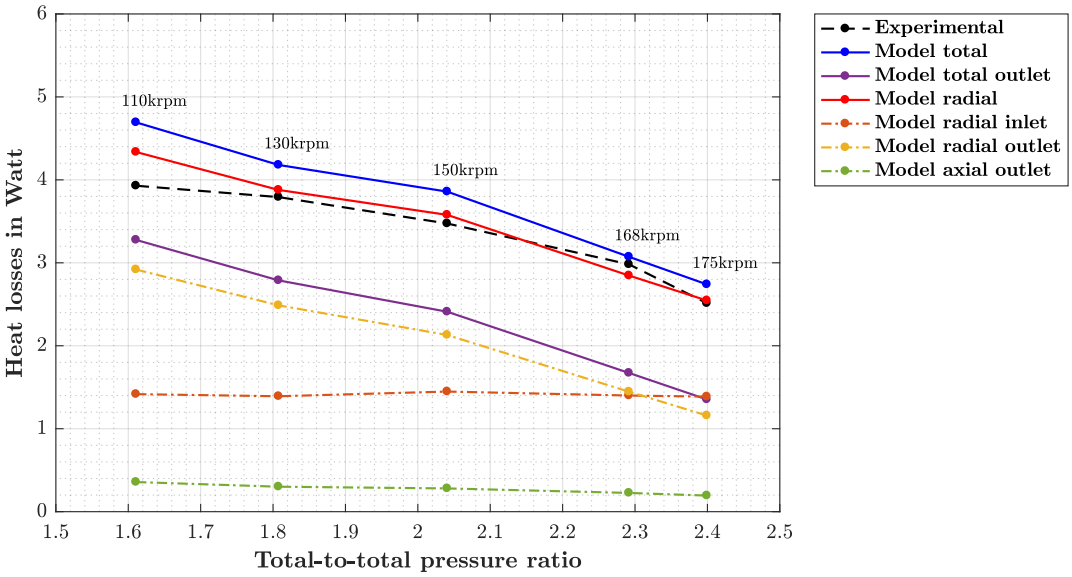

Figure 15: Heat losses of the turbine determined experimentally and computed using the model with respect to the total-to-total pressure

the outlet radial heat losses are more important than the axial losses. In fact, they represent 87% ± 2% of the modelled outlet turbine losses. Nonetheless, at the turbine outlet, the model underestimates the experimental heat losses by a range of 16% to 47%, with a 46.16% underestimation at 175krpm, the design rotational speed.

8 | Conclusion

The small-scale radial steam turbine was investigated using different approaches, based on thermodynamics laws, in order to determine its performance parameters. The turbine was investigated experimentally, numerically, analytically to evaluate its power, and its total-to-total isentropic efficiency.

First of all, an experimental investigation was conducted on the turbine based on several temperature and pressure measurements : the initial and the new measurements. The turbine was tested with cold ambient air, and with hot air entering the turbine at 220°C. The significant difference between the old and the new temperature measurements at the turbine outlet underlines the non-negligible impact of the heat transfers on the results.
The new measurements were used to update the boundary conditions of the turbine single-passage numerical model.
Moreover, an analytical investigation based on the Soderberg model [9] and the mean-line analysis was conducted on the turbine in order to estimate the isentropic total-to-static efficiency.

The analysis of the experimental, numerical and analytical results emphasises the challenge faced due to the influence of the heat transfers. In fact, the results of the various approaches lie within a relatively large range. Therefore, it is difficult to deduce exact values for the power and the isentropic total-to-total efficiency. However, it is possible to estimate an order of the power and the isentropic total-to-total efficiency of 34W and 39%, respectively.

Furthermore, a heat investigation of the FTU was conducted using a simplified model to evaluate the heat losses to the environment and localise their main sources. The modelled losses are compared to the heat losses determined experimentally. The model indicates that the main heat losses occur at the turbine, more precisely, at the turbine outlet.

As future work, a more rigorous heat investigation, which takes into account the measurement uncertainties, the mechanical losses, and the heat influence, can be conducted on the FTU. By evaluating the distribution of the heat dissipated by the mechanical losses throughout the FTU, it is possible the determine the heat transferred to the turbine and the fan, respectively, and therefore evaluate their powers and total-to-total isentropic efficiencies with more accuracy.

A | Recovery Factor of the Thermocouples

In a compressible flow, the recovery factor of the thermocouple should be taken into consideration. In fact, the kinetic energy of the fluid is not fully converted to thermal energy because of the viscous dissipation of the fluid and the heat losses by conductivity. The thermocouple recovery factor is defined as the ratio between the measured temperature and the total temperature of the fluid [13].

$$\lambda = \frac{T_{measured}}{T_t} \tag{47}$$

The recovery factor is smaller than 1, since the temperature measured is a value between the static temperature and the total temperature of the fluid.

The flow is subsonic and reaches a maximum Mach number of $M = 1$. The following correlations from Hirschberg [13] are used to evaluate the recovery factor, taking the fluid properties at the appropriate thermodynamic state.

$$\lambda = \begin{cases} 1 - 0.0070M^2 + 0.036M^4 & \text{if} \quad M < 1 \quad \text{and} \quad Re \approx 3 \times 10^3 \\ \\ \frac{1+(\frac{\gamma-1}{2})f(Pr,Re)M^2}{1+(\frac{\gamma-1}{2})M^2} & \text{if} \quad M < 0.6 \quad \text{and} \quad 100 < Re < 10^5 \\ f(Pr, Re) = \frac{4.3\times10^3+0.7Re}{4.3\times10^3+Re}Pr^{1/2} & \end{cases} \tag{48}$$

The Reynolds number is defined using the diameter (d_{TC}) of the thermocouple and the velocity of the fluid (u).

$$Re = \frac{\rho u d_{TC}}{\mu}$$

B | Mesh Sensitivity

In order to carry out numerical simulations rigorously, the first step is to determine the appropriate mesh sensitivity. The choice of the mesh is a compromise between the running time of the simulation and the accuracy of the results. In this case, an important parameter which has to be verified is the near wall element size y^+ value. In fact, on the rotor blades of the turbine, it is possible to have a flow separation. Consequently, y^+ has to be close to 1 so that this separation can be differentiated from the boundary layer.

The mesh sensitivity is selected by monitoring the numerical results of two performance parameters of the turbine, the power and the isentropic efficiency, with respect to the number of nodes. Moreover, the average y^+ value at the rotor blade is verified for each mesh.

The boundary conditions used for the following simulations are

- Total pressure at the inlet $p_{t,in} = 1.7975$bar
- Total temperature at the inlet $T_{in} = 215.9096$°C

- Static pressure at the outlet $p_{out} = 0.83$bar
- The rotational speed of the rotor $\Omega = 165.450$krpm

Since the efficiency of the turbine varies only slightly from one mesh to another as seen on Figure 17, the mesh will be chosen by analysing the results of the power of the turbine in Figure 16. Starting 0.6 million nodes, the values of the power are almost constant. Furthermore, the mesh with 0.6 million nodes presents an average $y^+ = 1.24$ close to 1 (Figure 18).

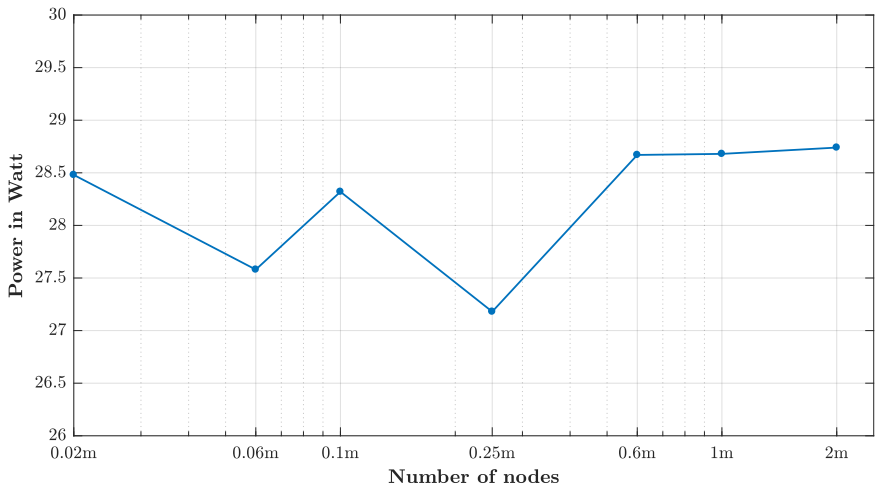

Figure 16: Power of the turbine for different meshes

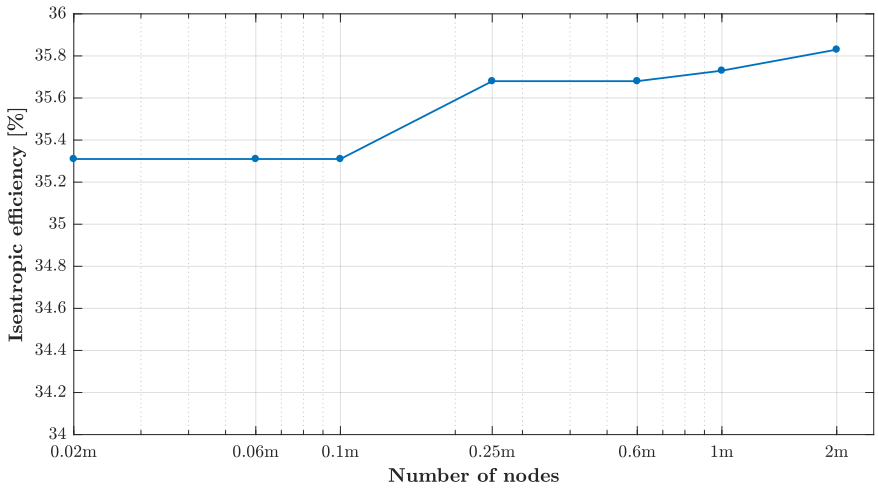

Figure 17: Isentropic efficiency of the turbine for different meshes

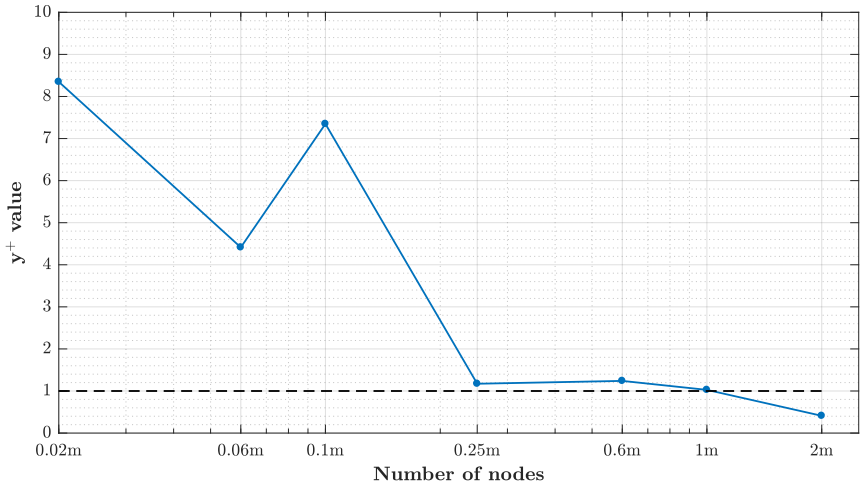

Figure 18: The average y^+ value at the rotor blade for different meshes

Therefore, the mesh with 0.6 million nodes is chosen. This mesh is selected since it provides satisfactory results as well as an adequate near wall element size. This simulation runs for a reasonable time, and increasing the number of nodes would lead to an unnecessary increase of the running time of the simulation.

Nomenclature

A	Area	[m^2]
H	Blade height	[m]
L	Length	[m]
M	Mach number	
P	Power	[W]
Pr	Prandtl number of the fluid	
Q	Heat transfer rate	[W]
Q_{loss}	Heat losses to the environment	[W]
R	Thermal resistance	[K W^{-1}]
Ra_D, Ra_L	Rayleigh number	
Re	Reynolds number of the flow	
T	Total temperature	[K]
$T_{measured}$	Measured non-corrected temperature	[K]
Ω	Rotational speed	[rpm]
α	Absolute blade angle based on the circumference	[rad]
α_f	Thermal diffusivity	[m^2 s^{-1}]
β	Relative blade angle based on the circumference	[rad]
β_f	Thermal expansion coefficient	[K^{-1}]
δ	Degree of reaction of the turbine	
$\dot{m}$	Mass flow rate	[kg s^{-1}]
η	Total-to-total isentropic efficiency	
γ	Heat capacity ratio of the fluid	
λ	Recovery factor	
μ	Dynamic viscosity of the fluid	[Ns m^{-2}]
ν	Kinematic viscosity of the fluid	[m^2 s^{-1}]
ω	Angular velocity	[rad s^{-1}]
$\overline{Nu}_D, \overline{Nu}_L$	Nusselt number	
ρ	Density of the fluid	[kg m^{-3}]
ζ	Loss coefficient	
c	Absolute velocity	[rad s^{-1}]
c_p	Specific heat capacity	[J kg^{-1}K^{-1}]
d	Diameter	[m]
h	Heat transfer coefficient	[W m^{-2}K^{-1}]

h_t	Total specific enthalpy	[J kg^{-1}]
k	Thermal conductivity	[W m^{-1}K^{-1}]
n	Number of blades	
p	Static pressure	[Pa]
p_t	Total pressure	[Pa]
r	Radius	[m]
s	Specific entropy	[J kg^{-1}K^{-1}]
t_{max}	Maximum blade thickness	[m]
u	Velocity of the fluid	[m s^{-1}]
x	Fraction of heat transferred to the turbine	
y^+	Average y^+ value of a mesh element	

Abbreviation

AOR	Anode Off-Gas Recirculation
CFD	Computational Fluid Dynamics
FTU	Fan-Turbine Unit
LE	Leading Edge
SOFC	Solid Oxide Fuel Cell
TE	Trailing Edge

Subscript

air	Air
amb	Ambient
ax	Axial
$blade$	Blade
CFD	Computational Fluid Dynamics
$conv$	Convection
exp	Experimental value of a quantity
f	Fiberglass tape
fan	Fan
FTU	Fan-Turbine Unit
hyd	Hydraulic
in	Inlet of the turbine
is	Isentropic
LE	Leading Edge
$mech$	Mechanical
$model$	Modelled quantity of a value

new	New measurements
old	Old measurements
out	Outlet of the turbine
rad	Radial
real	Real value of a quantity
rotor	Rotor
rs	Rotor-stator interface
s	Surface
shroud	Shroud of the turbine
stage	Stage of the turbine
steel	Steel
TC	Thermocouple
TE	Downstream of the trailing edge of the turbine
tot	Total
tst	Total-to-static
tt	Total-to-total
turb	Turbine
volute	Volute of the turbine

List of Figures

2 Small-scale radial steam turbine [1] 1
3 Turbine test rig and sensors 4
4 Temperature and pressure measurements locations (adapted from Wagner[1]) 5
5 k-Type thermocouples with a diameter of 0.15mm (left) and 1.5mm (right) . 6
6 Position of the two new thermocouples at the volute and downstream of the trailing edge 7
7 Microscope pictures of the new thermocouples at the volute (a) and downstream of the trailing edge (b) 7
8 Temperature measurements for the cold air test at different rotational speeds with respect to the total-to-total pressure ratio 8
9 Temperature measurements for the hot air test at different rotational speeds with respect to the total-to-total pressure ratio 9
10 CFD numerical model of a single-passage of the turbine 11
11 Performance results of the cold air test conducted on the turbine 15
12 Performance results of the hot air test conducted on the turbine 18
13 FTU simplified model for the heat transfer investigation 20
14 Heat losses determined experimentally and computed using the model with respect to the total-to-total pressure ratio 22
15 Heat losses of the turbine determined experimentally and computed using the model with respect to the total-to-total pressure 24
16 Power of the turbine for different meshes 27
17 Isentropic efficiency of the turbine for different meshes 27
18 The average y^+ value at the rotor blade for different meshes 28

List of Tables

1 Sensors used for the measurements 4
2 Temperature measurements 6

References

[1] Patrick Hubert Wagner. "Integrated Design, Optimization, and Experimental Realization of a Steam-Driven Micro Recirculation Fan for Solid Oxide Fuel Cell Systems". In: (2019), p. 261. DOI: 10.5075/epfl-thesis-9337.

[2] Prof. Dr. A. Bolcs and Dr. P. Ott. *Introduction aux turbomachines thermiques*. EPFL, Lausanne, 2019.

[3] Patrick Hubert Wagner et al. *Experimental Characterization of a Solid Oxide Fuel Cell Coupled to a Steam-Driven Micro Anode Off-Gas Recirculation Fan*. Journal of Applied Energy (accepted for publication).

[4] Mark Fernelius and Steven Gorrell. "Thermocouple Recovery Factor for Temperature Measurements in Turbomachinery Test Facilities". In: *52nd AIAA Aerospace Sciences Meeting - AIAA Science and Technology Forum and Exposition, SciTech 2014* (Jan. 2014). DOI: 10.2514/6.2014-0791.

[5] Bela Liptak. *Instrument Engineers' Handbook, Third Edition: Volume Three: Process Software and Digital Networks*. CRC Press, 2002.

[6] Conax Technologies. *Field Installation of Thermocouple & RTD Temperature Sensor Assemblies*. 2010. URL: https://www.conaxtechnologies.com/wp-content/uploads/2016/04/Conax_6027_FieldInstallation.pdf. (Accessed : 10.12.2019).

[7] National Institute of Standards and Technology. *NIST Reference Fluid Thermodynamic and Transport Properties Database (REFPROP)*. URL: https://www.nist.gov/srd/refprop.

[8] Marcos Font Armenteras. "Analytical and Numerical Investigation of a Small-scale Radial-Inflow Steam Turbine". In: (2019). URL: https://upcommons.upc.edu/handle/2117/134806.

[9] Soderberg, C. *Unpublished notes*. 1949. Gas Turbine Laboratory, MIT.

[10] Zweifel, O. *The spacing of turbomachine blading, especially with large angular deflection*. Brown Boveri Review,32, 12, 1945.

[11] Michael Ashby, Hugh Shercliff, and David Cebon. *Materials. Engineering, Science, Processing and Design*. Third Edition. ELSEVIER LIMITED, 2014.

[12] Incropera et al. *Fundamentals of Heat and Mass Transfer*. 6th Edition. John Wiley & Sons, 2007.

[13] A. Hirschberg and J.C. Van Mui Winke. *A Correlation of Recovery Temperature Data For Cylinders in a Compressible Flow at High Reynolds Numbers*. Department of Mechanical Engineering, Delft University of Technology, Delft, The Netherlands. Aug. 1976.